Energy transduction in the F_1 motor of ATP synthase

Hongyun Wang & George Oster

Department of Molecular and Cellular Biology, and College of Natural Resources, University of California, Berkeley, California 94720-3112, USA

ATP synthase is the universal enzyme that manufactures ATP from ADP and phosphate by using the energy derived from a transmembrane protonmotive gradient. It can also reverse itself and hydrolyse ATP to pump protons against an electrochemical gradient. ATP synthase carries out both its synthetic and hydrolytic cycles by a rotary mechanism[1–4]. This has been confirmed in the direction of hydrolysis[5,6] after isolation of the soluble F_1 portion of the protein and visualization of the actual rotation of the central 'shaft' of the enzyme with respect to the rest of the molecule, making ATP synthase the world's smallest rotary engine. Here we present a model for this engine that accounts for its mechanochemical behaviour in both the hydrolysing and synthesizing directions. We conclude that the F_1 motor achieves its high mechanical torque and almost 100% efficiency because it converts the free energy of ATP binding into elastic strain, which is then released by a coordinated kinetic and tightly coupled conformational mechanism to create a rotary torque.

The general structure of ATP synthase is shown in Fig. 1. It consists of two portions: a soluble component, F_1, containing the catalytic sites, and a membrane-spanning component, F_o, comprising the proton channel. The entire F_oF_1 structure is arranged as a counter-rotating 'rotor' and 'stator' assembly. The stator portion consists of the catalytic sites contained in the $\alpha_3\beta_3$ hexamer, together with subunits a, b_2 and δ. The rotor consists of 9–12 c-subunits arranged in a ring and connected to the γ- and ϵ-subunits that form the central 'shaft'. The mechanism of protonmotive force transduction has been discussed elsewhere[7]; we now focus on the mechanochemistry of F_1, which synthesizes ATP when the γ–ϵ shaft is turned clockwise (viewed from the membrane) by the protonmotive force, and which rotates counterclockwise to pump protons when hydrolysing ATP.

Any mechanism proposed to explain the experimental results is strongly constrained by thermodynamic, kinetic, structural and mechanical considerations. In the hydrolysis direction, it must reproduce the large torque and almost 100% mechanical efficiency[5,6]; in the synthesis direction, ATP must be produced at the measured rate when driven by torques generated by the protonmotive force in F_o. Kinetic constants and free energies must correspond to measured values. A model must also be geometrically compatible with the detailed structural information now available.

We constructed the model in three steps. First, kinematic motions of the F_1 subunits were analysed to determine the conformational changes that drive rotation of the γ-subunit. From this, we constructed a mathematical model describing the principal mechanical and electrostatic interactions between the subunits. Finally, the reaction sequences were incorporated to create a complete mechanochemical model. The outline of this model can be summarized as follows.

The reactivity of a catalytic site depends on its local conformation and composition. The unique feature of F_1 is that the reactivity of each site depends on the states of the other two sites, and the position of γ. Each of the three catalytic sites, β_1, β_2 and β_3, passes through at least four chemical states:

$$\underset{\text{Empty}}{\text{E}} \xrightarrow[\text{binding}]{\text{ATP}} \underset{\text{bound}}{\text{T}} \xrightarrow{\text{Hydrolysis}} \underset{\text{and } P_i \text{ bound}}{\text{D·P}} \xrightarrow[\text{release}]{P_i} \underset{\text{bound}}{\text{D}} \xrightarrow[\text{release}]{\text{ADP}} \underset{\text{Empty}}{\text{E}} \quad (1)$$

We denote by β_i the chemical state (E, T, D·P, D) of the ith β-subunit, so that $\alpha_3\beta_3$ has a total of $4^3 = 64$ possible kinetic states. The collection of these states can be visualized as the integer points in a $4 \times 4 \times 4$ cube (actually, a three-dimensional torus, because when the state exits one face of the cube, it re-enters the opposite face). The progression of the system through this chemical-state space depends on the angular position of the γ-subunit, which we denote by θ. The kinetics can be described by a set of equations (that is, a Markov model) of the form

$$d\beta_i/dt = K(\theta, \beta_{i-1}, \beta_{i+1}) \times \beta_i \quad (2)$$

where $i = 1, 2, 3$ and where K is the matrix of kinetic transition rates for a catalytic site, which depends on the angular position of γ and the occupancy of the other sites. Thus the state of F_1 is specified by its rotational position and its kinetic state: $(\theta, \beta_1, \beta_2, \beta_3)$.

The motion of γ is described by balancing the torques on the rotating γ-subunit:

$$\underbrace{\zeta \frac{d\theta}{dt}}_{\text{Viscous torque on } \gamma} = \underbrace{\tau(\theta, \beta_1, \beta_2, \beta_3)}_{\text{Torque between } \gamma \text{ and } \alpha_3\beta_3} - \underbrace{T_L}_{\text{Load torque}} + \underbrace{\mathcal{T}_B(t)}_{\text{Brownian torque}} \quad (3)$$

The viscous load on the rotating γ-subunit is contained in the drage coefficient, ζ. T_L represents any additional load torque (such as from a laser trap). $\mathcal{T}_B(t)$ is the brownian torque due to thermal fluctuations. The driving torques exerted on γ by the β-subunits can be expressed as the gradient of an elastic potential: $\tau(\theta, \beta_1, \beta_2, \beta_3) = -\partial V(\theta, \beta_1, \beta_2, \beta_3)/\partial\theta$. This potential is derived from the geometry

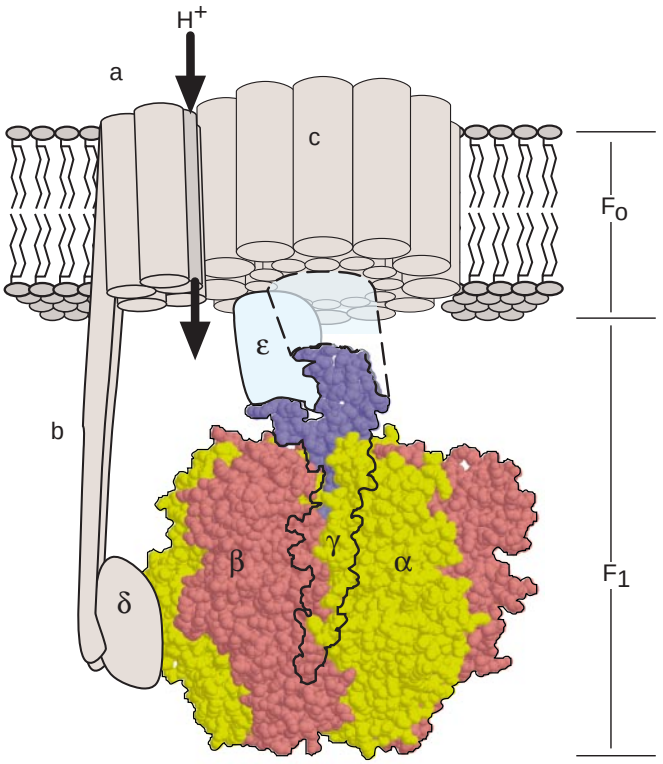

Figure 1 Structure of ATP synthase. It has a transmembrane portion, F_o, consisting of the stoichiometric subunits $c_{12}ab_2$, and a soluble portion, F_1, which consists of subunits $\alpha_3\beta_3\gamma\epsilon\delta$. Functionally, the protein behaves as a 'rotor' ($c_{12}\gamma\epsilon$) and a 'stator' ($ab_2\delta\alpha_3\beta_3$), which are thought to counter-rotate during hydrolysis and synthesis. The three catalytic sites are located at the αβ interfaces, and the proton channel is at the c–a interface. The dashed outline represents the fragment of γ that has not been resolved. In recent hydrolysis experiments[5,6], the $\alpha_3\beta_3$ subunit was attached to a coverslip and a fluorescently tagged actin filament was attached to the γ-subunit so that rotation of γ could be observed; here, only subunits $\alpha_3\beta_3\gamma$ were present.

and elastic properties of the mechanical model for F_1. We constructed this mechanical model by the following procedure.

First, we analysed the kinematic motions of F_1. To do this, we imported the coordinates for $\alpha_3\beta_3\gamma$ from the Protein Data Bank into the molecular structure program Rasmol[1,8]. According to Boyer's binding change mechanism, a $2\pi/3$ rotation of γ corresponds to a $2\pi/3$ advance in the kinetic states of the three catalytic sites and a $2\pi/3$ advance of the conformational asymmetry of the $\alpha_3\beta_3$ hexamer. This allows us to derive the coordinates of F_1 for $\theta = 2\pi/3$ from those at $\theta = 0$. For angles between 0 and $2\pi/3$, the coordinates of F_1 are calculated by interpolation in a cylindrical coordinate system. From this we created stereo animations of the complete motion of F_1 through the hydrolysis cycle (see Supplementary Information). Although the interpolated positions obey all steric constraints, they are probably not exact; nevertheless, they do give an idea of the overall motion of the subunits.

Next, we placed a local coordinate system on each subunit so that we could determine quantitatively the subunit's sequence of conformations. A study of the Protein Motions Database shows that most conformational changes can be resolved into hinge and shear motions[9,10]. The principal motion of the β-subunits consists of a hinge motion that bends the top and bottom segments towards one another by about 30° (Fig. 2), and two much smaller motions which we ignore: a radial shear motion and rotation in the θ direction. The α-subunits undergo very little change in shape.

To see how the vertical bending motion is converted into a rotary torque on the γ-subunit, we took horizontal 'serial sections' through the $\alpha_3\beta_3\gamma$ assembly to determine the cross-sectional shapes of γ and the central channel in $\alpha_3\beta_3$ into which γ fits. Combining this information, we deduced that the curved and asymmetric γ-subunit is driven by the hinge motion of the β-subunits in a fashion analogous to a hand on the crank of a car jack (see Supplementary Information).

We now make an important assumption about how the free energy from ATP hydrolysis is converted into the hinge-bending motion of β: the energy to bend a β-subunit is conferred on the catalytic site at the nucleotide-binding step in equation (1); that is, the rapid sequential bonding of the nucleotide to the catalytic site is converted into an elastic strain energy of $\sim 24\, k_BT$ ($14\ \mathrm{kcal\ mol^{-1}}$) centred at the catalytic site. Binding may proceed in several stages: for example, weak binding, followed by a rapid thermal 'zippering' of (mostly hydrogen) bonds—primarily to the phosphate groups. However, for simplicity we treat the binding as a single kinetic step in equation (1). This strain energy tends to bend the β-subunit, and the bending stress is converted by the protein's geometry into a rotary torque on the γ-subunit and to stresses on the other catalytic sites (Fig. 2).

Viewed as an elastic body, the $\alpha_3\beta_3$ hexamer is complicated, and certainly not isotropic. However, we can construct a simplified mechanical equivalent that captures its principal motions[11,12]. In this way, the complicated elastic behaviour of F_1 can be approximated by an assembly of rigid elements connected by springs (Fig. 2b).

We treat the $\alpha_3\beta_3$ hexamer as an elastic body with a pre-stress arising from the free energy of assembly. First, we model the intrinsic elasticity of the β-subunits as passive elastic elements at the hinge points. Second, we represent the active stress created by nucleotide binding as much stronger elastic elements that are activated upon nucleotide binding. Third, by assigning reasonable elastic constants to these elements (Box 1), we can compute elastic potential energies based on the simplified molecular structure shown in Fig. 2, one potential curve for each of the 64 kinetic

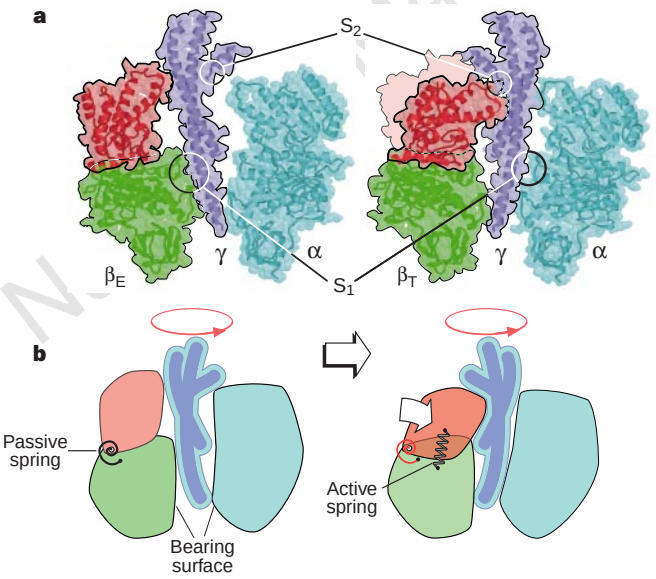

Figure 2 Conformation changes in the β-subunit. **a**, Side-view cross-section showing the conformational changes of the β-subunit in the empty (E) and ATP-bound (T) states, and the corresponding rotation of the γ-subunit as deduced from an analysis of the PDB coordinates (see Supplementary Information for procedures and animation moves). The two switch regions[14], denoted by S_1 and S_2, control nucleotide binding and phosphate release, respectively, at each catalytic site. **b**, Mechanical model used to compute the elastic potential that drive the rotation of the γ-subunit (described in Supplementary Information). The hinge-bending motion of β rotates the upper portion by ~30°. This is converted into a rotary torque on γ by the asymmetric bend in γ. The torque on γ is contributed by two β-subunits at a time, because each β has two free-energy drops during each hydrolysis cycle (Fig. 3a).

Box 1 Multisite reaction rates

Multisite reaction rates are constructed from the unisite rates by taking into account the effects of coupling of each catalytic site to the other sites, the two switches on the γ-subunit, and the elastic energy of each site. The elastic constants of the active and passive springs refer to Fig. 2.

Construction of the multisite reaction rate k^M from the unisite reaction rate k^U:

$$k^M_{\mathrm{forward}}(\theta, \beta_{i-1}, \beta_{i+1}) = k^U_{\mathrm{forward}} \times f(\beta_{i-1}, \beta_{i+1}) \times g(\theta) \times \exp\left(\frac{\lambda \times \Delta E(\theta)}{k_BT}\right)$$

$$k^M_{\mathrm{backward}}(\theta, \beta_{i-1}, \beta_{i+1}) = k^U_{\mathrm{backward}} \times f(\beta_{i-1}, \beta_{i+1}) \times g(\theta) \times \exp\left(\frac{-(1-\lambda) \times \Delta E(\theta)}{k_BT}\right)$$

$f(\beta_{i-1}, \beta_{i+1})$ contains the effect of the occupancy of other sites. Binding of ATP on other sites increases the reaction on this site. $g(\theta)$ models the effect of switches S_1 and S_2: rotation of γ brings the switch regions on β and γ into proximity, which increases the reaction rate. $\Delta E(\theta)$ is the elastic energy difference between the two chemical states of β. (see Supplementary Information).

Elastic constants of active and passive springs:

$$k_{\mathrm{active}} = 10\ \mathrm{pN\,nm^{-1}},\ \text{and}\ k_{\mathrm{passive}} = 4\ \mathrm{pN\,nm^{-1}}.$$

The active and passive springs are pre-compressed by 4 nm. During hydrolysis, the additional displacement of these springs is 2 nm.

states. The derivatives of these elastic potentials yield the torques that drive the rotation of γ, as given in equation (3).

The exact procedure for constructing the potentials is given in the Supplementary Information. Roughly, this consists of measuring the bending motions of a β-subunit by the azimuthal angle, ϕ, between its upper and lower portions. During the course of its conformational change, a β-subunit closes and opens its azimuthal angle by about $\Delta\phi \approx 30°$. Trigonometry yields a relationship between the bending angle, ϕ, of a β-subunit and the rotation angle of γ : $\theta = f(\phi)$. As the bending angle ϕ closes, β pushes on the off-axis bowed segment of γ (Fig. 2). In this way, a rotary torque in the θ direction is generated by the geometric propagation of stress from the catalytic site (the active spring) to γ. As each of the subunits cycles through its conformational range in sequence, a continuous rotational torque is exerted on γ.

The unisite (that is, at substoichiometric ATP concentration) rate constants for the transitions given in equation (1) have been measured[13]. But, at steady state the reactions at the three catalytic sites are coordinated in two ways. First, the strain induced by nucleotide binding at each site is communicated to the other two sites. Second, there are at least two 'switch points' on γ that interact with specific sites on the $\alpha_3\beta_3$ hexamer[14]. Thus, the activation energy barriers for the reaction at each site are influenced by the state of the other two sites and the angular position of the γ-subunit.

Figure 3a shows the free-energy levels of a β-subunit as the system evolves through the 64 possible chemical states. Note that, as measured externally, only part of the free energy of ATP is released to the surroundings upon binding: the remainder is stored internally as elastic deformation and released when phosphate is released. The switch denoted by S_1 in Figs 2 and 3 is located at γGln 269 and

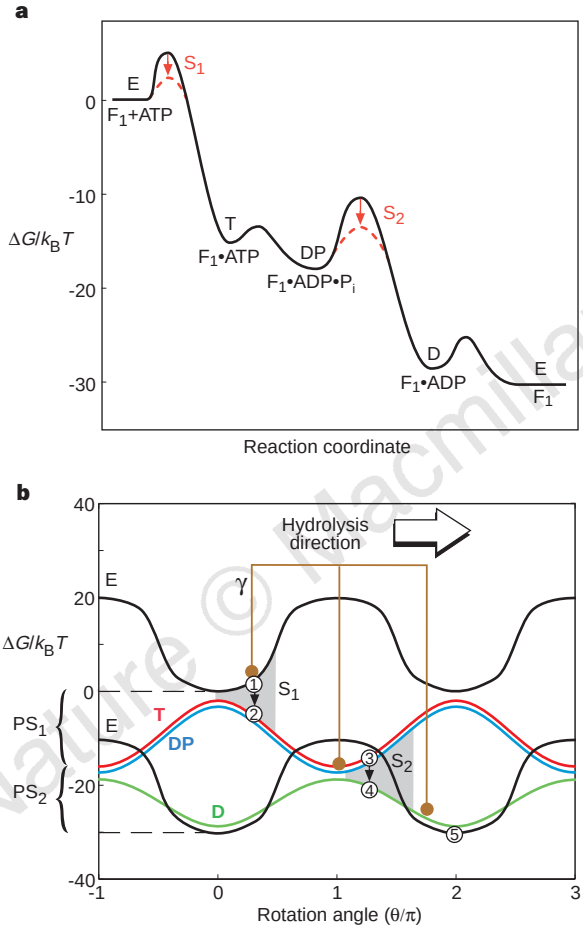

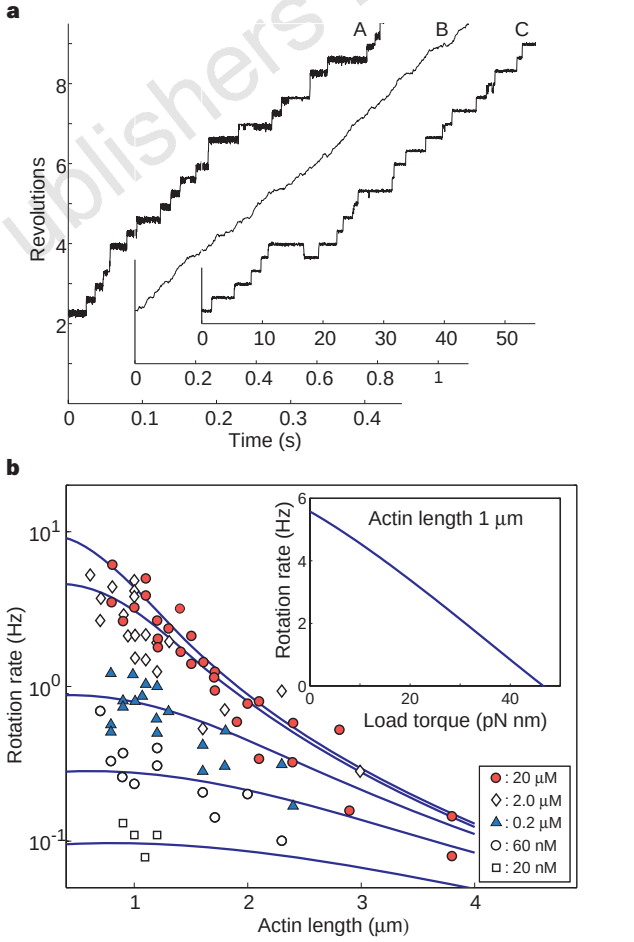

Figure 3 Energy profiles. The free energy of F_1 during its hydrolysis cycle depends on the chemical state of each β-subunit, represented by β_i = (E, T, DP, D), and the angular coordinate, θ, of the γ-subunit: $\Delta G(\theta,\beta_1,\beta_2,\beta_3)$. **a**, Projection of the free energy onto the reaction coordinate of a single β-subunit. The free-energy drop proceeds in 4 stages (see equation (1)). The free-energy drops are computed from unisite reaction rates (the free-energy barriers are shown schematically). The transition E → T (nucleotide binding) is activated by switch S_1; the transition DP → D (phosphate release) is activated by switch S_2. **b**, Free-energy profile of the interaction between the γ-subunit and a single β-subunit, showing the 4 elastic periodic potentials along which the system is constrained to move. Numbers trace the trajectory of a catalytic site through one cycle of hydrolysis, which generates two power strokes. The primary power stroke (PS_1) occurs upon binding of nucleotide, which drives the bending of the β-subunit. During this bending, the elastic stress turns γ and compresses the passive elastic element. The secondary power stroke (PS_2) is triggered by the release of phosphate, causing the elastic energy stored from the primary power stroke to be liberated during the first power stroke of the next site in the sequence.

Figure 4 Model predictions. **a**, Simulated rotational trajectories of the γ-subunit relative to $\alpha_3\beta_3$ at three different ATP concentrations and viscous loads. Trajectory A shows the rotation of γ when the ambient ATP concentration is 2 mM. The motor stochastically steps in increments of $2\pi/3$, and the rate is limited by ADP release. In trajectories B and C, a drag coefficient equivalent to an actin filament 1 μm long was imposed on the γ subunit[5,19]. Trajectory B corresponds to an ATP concentration of 2 mM. Here the viscous damping of the actin filament obscures the stepping behaviour. Trajectory C shows that the stepping behaviour reappears, even with the drag of the actin filament, when ATP drops to 20 nM. In this situation, hydrolysis is limited by diffusion of ATP to a catalytic site. Note that rare backward steps occur when nucleotide occasionally binds to the 'wrong' site. The average velocities are as measured in ref. 19. **b**, The rotation rate of γ when subjected to viscous loads from a long actin filament. Data points are from ref. 19. Solid lines are computed from the model, and fit the data at all loads and ATP concentrations. If an additional static load is imposed on a 1-μm actin filament from, say, a laser trap, the predicted load–velocity relation is shown in the inset.

βThr 304 (*Escherichia coli* sequence numbering); it activates binding of nucleotide successively to each catalytic site. The switch at γArg 242 and βGlu 381 of the conserved DELSEED sequence in the β-subunit (S_2 in Figs 2, 3) activates release of phosphate at each site. The interactions between the γ- and the β-subunits at the switch regions are electrostatic and are communicated to the catalytic sites to produce entropic and steric effects that do not involve appreciable changes in free energy.

From the configurational geometry and elastic constants, we can compute the sequence of elastic potentials the γ-subunit experiences from a β-subunit as it undergoes its cycle of nucleotide binding, hydrolysis and product release (Fig. 3b). The elastic energy curves of the other two β-subunits are identical to those shown, but shifted by $2\pi/3$ and $-2\pi/3$ respectively. The potential experienced by γ from the three driving β-subunits is the sum of these three sets of potentials. In Fig. 3b, this is represented by the three connected points (offset by $2\pi/3$) on one set of potentials. At one site, the cycle proceeds as indicated by the numbers 1–5, starting where the empty site binds ATP. This drops the state from point (1) on E to point (2) on T; this transition is triggered by S_1. The exact angle, θ, at which ATP binds is stochastic; the vertical arrow in Fig. 3b indicates a typical transition point; the binding of nucleotide strains the catalytic site, and release of this stress through the mechanical escapement shown in Fig. 2 rotates the γ shaft from (2) → (3). This is the primary power stroke. Approximately 180° opposite S_1 on γ is the second switch S_2, which triggers the release of phosphate (the transition from point (3) on DP to point (4) on D in Fig. 3b), initiating the secondary power stroke. The energy drop from (4) → (5) on the D curve in Fig. 3b releases the elastic strain stored during the primary power stroke. This takes place during the primary power stroke of the next site. Thus, each $2\pi/3$ rotation of γ is driven by two βs: the binding of nucleotide to one β and the release of elastic strain from the previous β when phosphate is released.

All that remains to complete the model is to specify the chemical rates, $K(\theta, s)$, in equation (2), which control the transition between the 64 different elastic potentials. The transition rates are determined by the free energy difference and the energy barrier between adjacent states. As already discussed and summarized in Box 1, the activation energy barrier of a catalytic site is affected by the chemical state of the other two sites and the interaction with the two switch regions on γ (see Supplementary Information for a complete description of the mathematical model and its numerical simulation). The results of these computations are summarized in Fig. 4.

Figure 4a shows typical trajectories for various ATP concentrations and viscous loads. At saturated ATP concentrations (2 mM) and with no additional viscous load, the motor rates in steps of $2\pi/3$, consuming one ATP per step (curve A). The rate-limiting step under these conditions is the release of ADP[15]. At low ATP concentrations, and with a large viscous load imposed by the actin filament attached to the γ-subunit[5,6], the motor also behaves as a stepper (curve C in Fig. 4a). In this situation, the motor is limited by the diffusion of ATP to the catalytic sites[16]. At high ATP concentrations and loads, the step-like progression of the motor is obscured by the viscous drag (curve B in Fig. 4a). At low ATP concentrations, the motor occasionally executes backward steps when nucleotide binds to the 'incorrect' site (curve C in Fig. 4a). These curves reproduce quantitatively the measurements of Yasuda *et al.*[6]. The mechanical efficiency of the motor—computed as the ratio of the average viscous dissipation per step to the free energy of hydrolysis—is very high, approaching 100% for large viscous loads. This high efficiency is possible because the motor is not a heat engine, but is driven almost completely by elastic strain energy.

Figure 4b shows the expected load–velocity relation, together with the velocity as a function of the length of an attached actin filament[5,6]. The motor can generate torques of more than 40 pN nm. The mechanical escapement allows the motor to release the strain energy conferred by nucleotide binding in two stages. The primary power stroke begins immediately upon nucleotide binding. This power stroke performs two tasks: it drives the γ-subunit in a full $2\pi/3$ rotation, and it also compresses the passive elastic element, storing nearly half of the elastic energy of binding. This elastic energy is released in a secondary power stroke that assists the next hydrolysis site during its primary power stroke. This two-stage release of stored energy smoothes the output torque and contributes to the high mechanical efficiency of the motor.

The model has three other predictions (see Supplementary Information): (1) it correctly predicts the measured rates of ATP synthesis when driven in reverse by a torque corresponding to that generated in F_o (refs 2, 17); (2) the proton flux through F_o coupled to the rotation of γ is blocked by small concentrations of ADP but then increases under normal synthesis conditions, in accordance with results from 'slip' experiments[18]; and (3) the average occupancy of the catalytic sites as a function of ATP concentration agrees well with experiments[13].

In summary, the model contained in equations (1)–(3) can quantitatively explain the principal features of the F_1 motor. The motor rotates in steps of $2\pi/3$, generating up to 45 pN nm of torque and consuming, on average, a single ATP per step, with a mechanical efficiency approaching 100%. To perform in this way, the motor cannot operate as a heat engine but converts the free energy of nucleotide binding into elastic strain energy. This strain energy drives the rotation of the γ-subunit through a tightly coupled mechanical mechanism, which is closely coordinated with the kinetic transitions. The general features of energy transduction in F_1 may have implications for other protein motors driven by nucleotide hydrolysis. □

Received 8 June; accepted 11 September 1998.

1. Abrahams, J., Leslie, A., Lutter, R. & Walker, J. Structure at 2.8 Å resolution of F_1-ATPase from bovine heart mitochondria. *Nature* **370,** 621–628 (1994).
2. Boyer, P. The binding change mechanism for ATP synthase—some probabilities and possibilities. *Biochim. Biophys. Acta* **1140,** 215–250 (1993).
3. Fillingame, R. H. Coupling H^+ transport and ATP synthesis in F_1F_o-ATP synthases: glimpses of interacting parts in a dynamic molecular machine. *J. Exp. Biol.* **200,** 217–224 (1997).
4. Cross, R. & Duncan, T. Subunit rotation in F_oF_1-ATP synthases as a means of coupling proton transport through F_o to the binding changes in F_1. *J. Bioen. Biomembr.* **28,** 403–408 (1996).
5. Noji, H., Yasuda, R., Yoshida, M. & Kinosita, K. Direct observation of the rotation of F_1-ATPase. *Nature* **386,** 299–302 (1997).
6. Yasuda, R., Noji, H., Kinosita, K., Motojima, F. & Yoshida, M. Rotation of the γ subunit in F_1-ATPase: Evidence that ATP synthase is a rotary motor enzyme. *J. Bioen. Biomembr.* **29,** 207–209 (1997).
7. Elston, T., Wang, H. & Oster, G. Energy transduction in ATP synthase. *Nature* **391,** 510–514 (1998).
8. Shirakihara, Y. *et al.* The crystal structure of the nucleotide-free α3 β3 subcomplex of F_1-ATPase from the thermophilic *Bacillus* PS3 is a symmetric trimer. *Structure* **5,** 825–836 (1997).
9. Gerstein, M., Lesk, A. & Chothia, C. Structural mechanisms for domain movements in proteins. *Biochemistry* **33,** 6739–6749 (1994).
10. Gerstein, M. in *Protein Motions* (ed. Subbiah, S.) 81–90 (Chapman and Hall, New York, 1996).
11. Alberts, B. The cell as a collection of protein machines: preparing the next generation of molecular biologists. *Cell* **92,** 291–294 (1998).
12. Rojnuckarin, A., Kim, S. S. & Subramaniam, S. Brownian dynamics simulations of protein folding: access to milliseconds time scale and beyond. *Proc. Natl Acad. Sci. USA* **95,** 4288–4292 (1998).
13. Senior, A. Catalytic sites of *Escherichia coli* F_1-ATPase. *J. Bioen. Biomembr.* **24,** 479–483 (1992).
14. Al-Shawi, M. & Nakamoto, R. Mechanism of energy coupling in the F_oF_1-ATP synthase: the uncoupling mutation, γM23K, disrupts the use of binding energy to drive catalysis. *Biochemistry* **36,** 12954–12960 (1997).
15. Hasler, K., Engelbrecht, S. & Junge, W. Three-stepped rotation of subunits γ and ϵ in single molecules of F-ATPase as revealed by polarized, confocal fluorometry. *FEBS Lett.* **426,** 301–304 (1998).
16. Yasuda, R., Noji, H., Kinosita, K. & Yoshida, M. F_1 ATPase is a stepper motor. *Biophys. J.* **74,** A1 (1998).
17. Matsuno-Yagi, A. & Hatefi, Y. Kinetic modalities of ATP synthesis: regulation by the mitochondrial respiratory chain. *J. Biol. Chem.* **261,** 14031–14038 (1986).
18. Groth, G. & Junge, W. Proton slip of the chloroplast ATPase: its nucleotide dependence, energetic threshold, and relation to an alternating site mechanism of catalysis. *Biochemistry* **32,** 8103–8111 (1993).
19. Yasuda, R., Noji, H., Kinosita, K. & Yoshida, M. F_1-ATPase is a highly efficient molecular motor that rotates with discrete 120° steps. *Cell* **93,** 1117–1124 (1998).

Supplementary information is available on *Nature*'s World Wide Web site (http://www.nature.com) or as paper copy from the London editorial office of *Nature*.

Acknowledgements. We thank J. Walker for discussions on the motions of the β-subunit and for videos of the three configurations which simulated our interpolated videos; R. Nakamoto for advice on the switch 1 and 2 interactions; M. Yoshida, K. Kinosita and their co-workers for inspiring the construction of the F_1 model by their ingenious experiments; and M. Grabe and K. Kinosita for insightful comments and suggestions on the manuscript.

Correspondence and requests for materials should be addressed to G.O. (e-mail: goster@nature.berkeley.edu).